J. Fluid Mech. (1982), *vol.* 117, *pp.* 269–282
Printed in Great Britain

The lateral wave at a depth discontinuity in the ocean and its relevance to tsunami propagation

By D. R. KING AND P. H. LEBLOND
Department of Oceanography, University of British Columbia, Vancouver, Canada

(Received 14 June 1979 and in revised form 15 September 1981)

The theory of lateral waves is reviewed in the context of long surface gravity waves and is used to interpret the results of experiments performed in a wave tank to simulate tsunami propagation following a disturbance on a continental shelf. It is suggested that since the lateral wave precedes the direct wave at coastal stations its detection might prove useful in tsunami warning systems.

1. Introduction

Large-scale sudden deformations of the sea floor generate trains of long surface gravity waves, known as tsunamis, which propagate into far corners of the ocean and may cause damage in areas too remote to be affected by the original tectonic event that gave birth to the tsunami. Far from the source, tsunami properties are determined by the characteristics of the generation mechanism, by refraction and dispersion along the propagation path, and by details of the coastal response; the subject has been extensively reviewed by Murty (1977). Tsunamis are commonly generated on or near shallow continental shelves; the early stages of their propagation may then be affected by the proximity of the steep continental rise. This paper examines the influence of the continental rise, idealized as a depth discontinuity, on the propagation of long waves on a shallow shelf. Particular emphasis is placed on the description of the *lateral wave* which arises at the discontinuity. This emphasis is motivated in part by the lack of general familiarity with this wave component in the water-wave context and also by the fact that the lateral wave is the first wave to arrive at remote shore locations, which may make it useful as a warning signal for the main tsunami waves which follow it.

The theory of lateral waves is reviewed in § 2, and basic results relevant to the shallow-water long gravity wave system are quoted from the analysis of King (1978). The experimental apparatus used to study the lateral waves is described in § 3 and the results obtained in it are presented in § 4. Applicability and relevance to tsunami warning are discussed in § 5.

2. The lateral wave

Consider a rectilinear continental shelf strip of depth h_1, bounded on one side by a non-reflecting shore and on the other by a depth discontinuity to a deep ocean basin of depth $h_2 > h_1$. An extensive axisymmetric sea-level perturbation on the shelf occurs impulsively and generates a train of shallow-water surface gravity waves. These waves

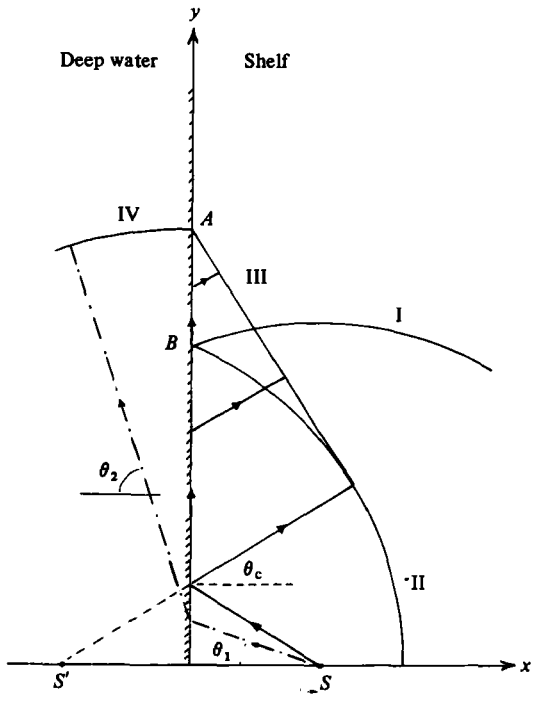

FIGURE 1. Wavefronts propagating from an impulsive symmetric source situated at S on a shallow shelf adjacent to a deep ocean. The direct wavefront (I) is centred on S; the reflected wave (II) seems to emanate from an image source at S'. A deep-water refracted wavefront (IV) and the lateral wavefront (III) complete the picture. Only selected rays are shown; one sub-critical direct ray ($\theta_1 < \theta_c$) and its refracted continuation ($\theta_2 < \frac{1}{2}\pi$) are represented by the dot–dash line. The solid-line rays all contribute to the lateral wave.

propagate on the shelf as a circular wavefront travelling at speed $c_1 = (gh_1)^{\frac{1}{2}}$. As the coast has been assumed to be fully absorbing, no complicating reflected waves arise when the wavefront hits the shore. At the depth discontinuity, simple geometrical optics shows that the incident waves are partly reflected, partly refracted into the deep-ocean region. The reflected waves travel back onto the shelf at speed c_1 as if they had been generated at an image source across the discontinuity (figure 1). Refracted rays are deflected from their original direction on the shelf according to Snell's law: $\sin\theta_2/\sin\theta_1 = (h_2/h_1)^{\frac{1}{2}}$. Since $h_2 > h_1$ total reflection occurs for

$$\theta_1 \geqslant \theta_c = \arcsin(h_1/h_2)^{\frac{1}{2}};$$

for angles beyond the critical angle θ_c, geometrical optics predicts that no wave energy enters the deep basin from the source at S on the shelf. A more precise analysis shows, however, that for $\theta_1 > \theta_c$ there is a wave on the deep-water side, with amplitude decaying exponentially from the discontinuity and travelling along it at the speed $c_2 = (gh_2)^{\frac{1}{2}}$. With reference to figure 1, we thus note that, at a point A along the depth discontinuity for which $\theta_1 > \theta_c$, wave energy first arrives at the deep-ocean speed c_2 in the form of the critically refracted wave propagating along the boundary (wave-front IV), before any direct wave travelling at the lower shelf-wave speed c_1 (which reaches point B when the refracted wave reaches A). For all points along the dis-

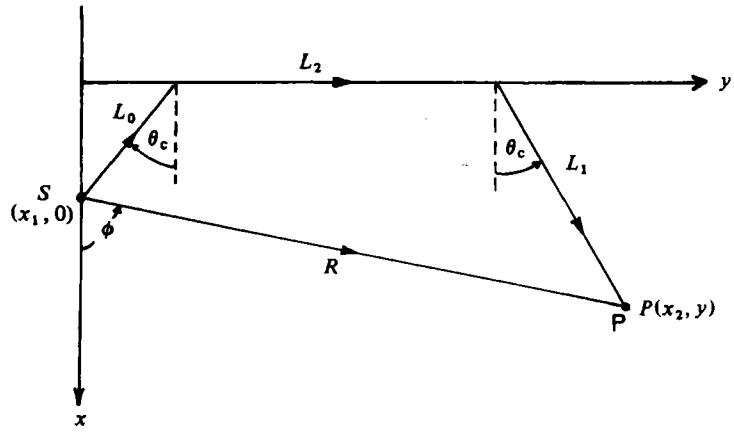

FIGURE 2. Travel paths to a remote observation point P from the source S. The direct wave travels a distance R in a straight line between the two points. The path of the lateral wave consists of the three segments L_0, L_2 and L_1. The path of the specularly reflected ray is not shown.

continuity between B and A in figure 1, the wave disturbance first arrives from the deep-water side and acts as a source of radiation for the shelf region: this is the source of the *lateral wave*. Since the lateral wave travels at speed c_1 on the shelf, its wavefront (III, in figure 1) must make an angle θ_c with the depth discontinuity in order to keep up with the deep-ocean wave travelling at speed $c_2 > c_1$.

To sum up, waves arising from the original impulse, as labelled in figure 1, include a direct (I) and a reflected (II) wave spreading radially on the shelf at speed c_1 from centres at S and S' respectively, a deep-ocean wave (IV) travelling at speed c_2, and a lateral wave (III) diffracted back onto the shelf by the deep-ocean wave but travelling at speed c_1 at an angle to the discontinuity. The lateral wave has been studied extensively in seismology, where it is also known as a 'head wave' or as a 'refraction arrival' and forms an important diagnostic tool in exploration geology (Heelan 1953). Detailed theoretical presentations of the origin and properties of lateral waves in elastic media are given by Cagniard (1939) and Brekhovskikh (1960). The theoretical framework used by Brekhovskikh has been applied by King (1978) to the study of long-gravity-wave propagation near a depth discontinuity in a rotating ocean; only results pertinent to a discussion of tsunamis, where the rotation of the Earth may be neglected, and to a comparison with small-scale model observations are quoted below.

What makes the lateral wave of particular interest is the fact that, at sufficiently great distances from the source, it may be the first signal to reach a distant observer. Let us consider a point of observation P located at (x_2, y) on the continental shelf (figure 2). The time t_D for the direct wave to reach P from a source S at $(x_1, 0)$ is

$$t_D = R/c_1, \tag{1}$$

with $R^2 = (x_2 - x_1)^2 + y^2$. The reflected wave clearly arrives later since it travels at the same speed over a longer path. The lateral-wave ray path first follows a direct ray at the critical angle for a distance $L_0 = x_1/\cos\theta_c$, then along the depth discontinuity for a distance $L_2 = y - (L_0 + L_1)\sin\theta_c$, and finally along a lateral wave ray for $L_1 = x_2/\cos\theta_c$. The segment along the discontinuity is covered at speed c_2; the

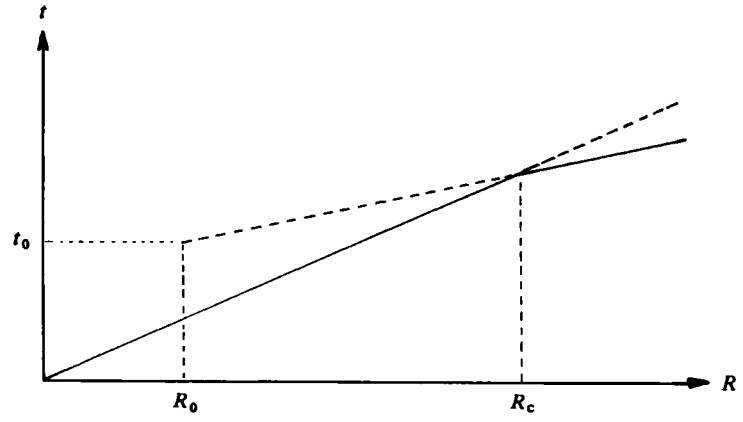

FIGURE 3. Time of first arrival (solid line) at a distant observation point as a function of the radial distance R from the source. The direct wave arrives first up to $R = R_c$, beyond which the lateral wave comes first.

other two segments at speed c_1. The lateral wave thus reaches the point P in a time

$$t_L = \frac{L_0 + L_1}{c_1} + \frac{L_2}{c_2}. \tag{2}$$

Substituting in terms of the co-ordinate values and for θ_c,

$$t_L = \frac{R \sin\phi}{c_2} + \frac{(x_1 + x_2)(c_2^2 - c_1^2)^{\frac{1}{2}}}{c_1 c_2}. \tag{3}$$

The lateral and direct wavefronts arrive simultaneously at a distance R_c, for which $t_D = t_L$, given by

$$R_c = \frac{(x_1 + x_2)(c_2^2 - c_1^2)^{\frac{1}{2}}}{c_2 - c_1 \sin\phi}. \tag{4}$$

A plot of first arrival time against distance (solid line in figure 3) shows that for $R < R_c$ the first response is due to the direct wave, but that at $R = R_c$ the lateral-wave and direct-wave arrival times cross over and that the lateral wave is the first arrival at $R > R_c$. For $L_2 = 0$, i.e.

$$R \leqslant R_0 = \frac{c_1(x_1 + x_2)}{\sin\phi (c_2^2 - c_1^2)^{\frac{1}{2}}}, \quad t < t_0 = \frac{(x_1 + x_2) c_2}{c_1 (c_2^2 - c_1^2)^{\frac{1}{2}}},$$

there is no lateral wave present. Reflected waves arrive at $R = R_0$, which is at the junction of the reflected and lateral wavefronts, along a ray reflected at the critical angle θ_c; for $R < R_0$, the rays are reflected at angles smaller than θ_c.

Sufficiently far from the source, and in the absence of damping, the amplitude of the direct wave decays as $\eta_D \propto R^{-\frac{1}{2}}$. The amplitude of the lateral wave decays as $\eta_L \propto L_2^{-\frac{3}{2}}$; at large distances $L_2 \to R$ and $\eta_L \propto R^{-\frac{3}{2}}$. Thus, although it may arrive first, the lateral wave will be appreciably smaller in amplitude than the direct wave which follows it.

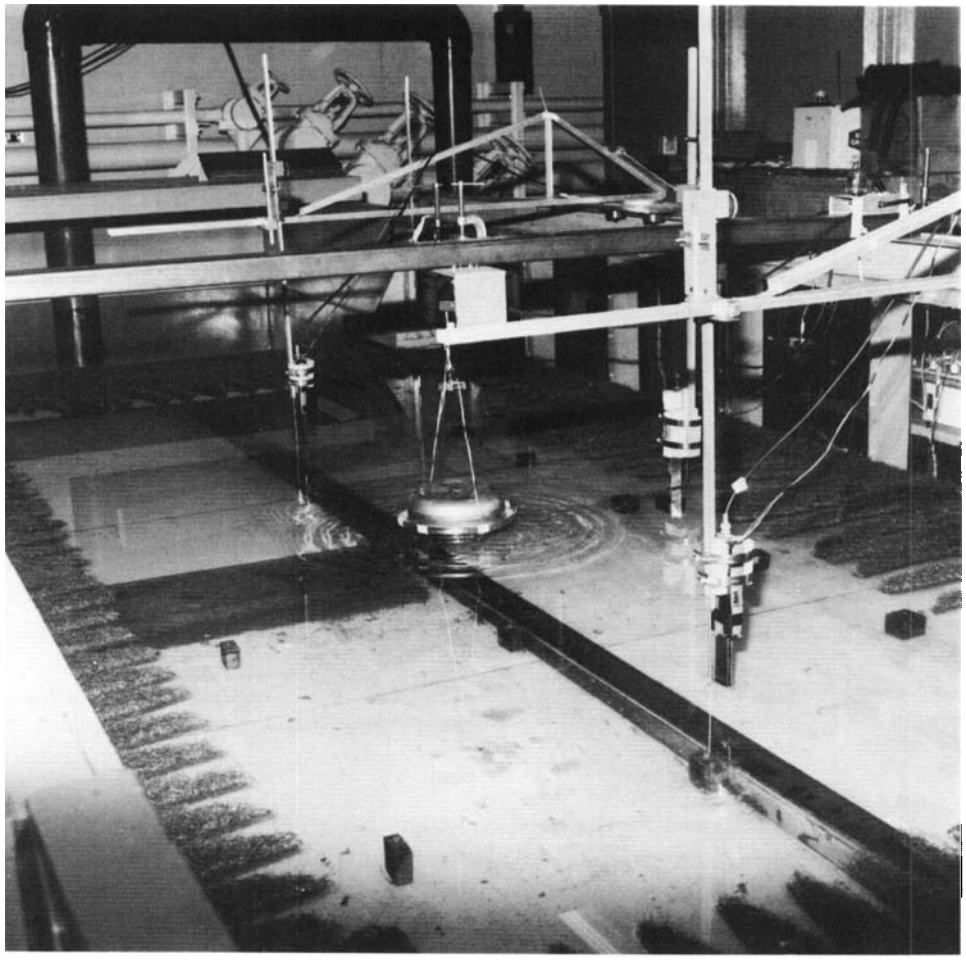

FIGURE 4. Overview of the wave tank, operating according to procedure (*a*), with the deep water in the forward left quadrant. The source is located near the centre; the three detectors are visible in the shallow-water region.

3. Experimental apparatus

Tsunami generation and propagation in the presence of an idealized continental-shelf structure was investigated experimentally in a small-scale model, with the purpose of verifying the adequacy of the theoretical results, especially with regard to the properties of the lateral wave.

The laboratory model used in the experiments was constructed within a wave tank of rectangular plan shape. A photograph of the wave tank with wave-generating and measuring apparatus and lateral damping baffles in place is shown in figure 4. The bottom area of the wave tank was divided into two domains: a permanent shelf region, and a region with a vertically positionable bottom which could be adjusted to the two configurations used in the study without changing the water level in the tank. Results reported here are for a shelf depth $h_1 = 1{\cdot}28$ cm and a 'deep-ocean' depth $h_2 = 2{\cdot}19$ cm. The ratio h_1/h_2 is not representative of that encountered between continental-shelf and deep-ocean regions in nature (where h_1/h_2 is typically 1/20). The depths chosen

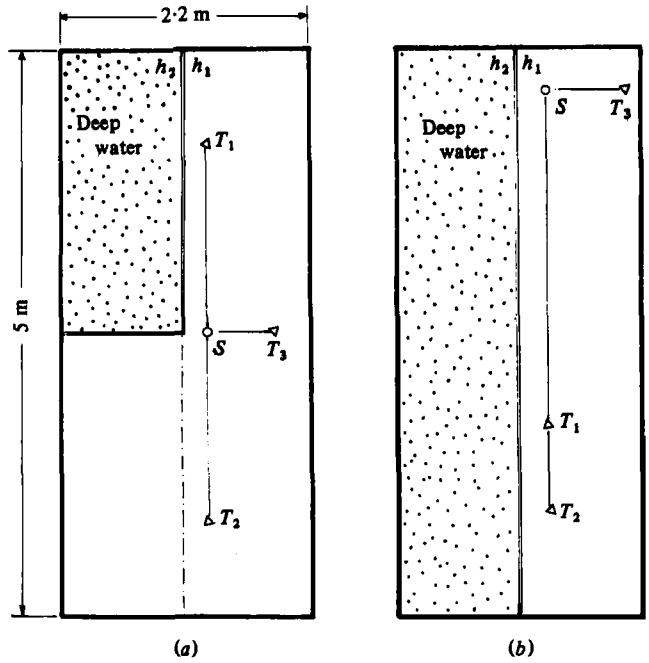

FIGURE 5. Plan views of the two basin configurations for the two experimental procedures (*a*) and (*b*) described in the text. The wave-source location is at S and detectors are placed at T_1, T_2 and T_3.

in the model were imposed by the need to satisfy the shallow-water conditions, the desire to resolve the lateral wave from the direct signal, and the physical dimensions of the tank. Shelf and deep regions were separated by a vertical discontinuity in depth. The side walls of the tank were lined with a saw-tooth pattern of horsehair packing material which effectively removed reflections; the configuration chosen was inspired by that used by Pite (1973) and is visible in figure 4.

Waves were generated on the shelf by a radially symmetric source consisting of an inverted vegetable steam-basket of diameter 12·5 cm. The source was activated in an impulsive mode by a solenoid which caused the leaves of the steamer to be suddenly extended and so to create a circularly symmetric wave disturbance. Measurement of the wave field was accomplished with three parallel-plate capacitance-type water-level detectors; all three of these are visible in figure 4. Two of the detectors were movable, suspended from a truss and carriage arrangement, and could be positioned at any point of interest within the tank; the third detector was stationary and was used to monitor the wave source. Details of the calibration of the detectors, of tests of the efficiency of the anti-reflecting baffles, of the operation of the wave source and of the signal-handling procedure after wave detection are documented in King (1978).

Two experimental procedures were followed to study the waves issuing from the source and their modification by the presence of the depth discontinuity. In the first configuration (*a*), the source was located near the centre of the tank (as shown in figure 5*a*), and measurements were first made under conditions of uniform depth h_1 at detectors T_1 and T_2 symmetrically placed on either side of the source along a line, on the shelf side, parallel to the shelf/deep ocean boundary. Under this arrangement,

only the direct wavefront (labelled (I) in figure 1) was generated. The positioning of detectors T_1 and T_2 was finely adjusted so that the direct wave arrived simultaneously at both; the gains of both detectors were also adjusted so that exactly the same signal would be recorded at the two positions. After this preliminary step, one quadrant of the tank floor was lowered to a depth h_2 (figure 5*a*). Waves recorded at detector T_1 would then include a direct, a reflected and a lateral wave. With gains as priorly adjusted, the direct wave was subtracted from the output of T_1 by taking away from it that of T_2, which recorded only a direct wave. The experiments were repeated with increasing separation of the detectors from the source.

The maximum distance from the source along the shelf where the reflected and lateral waves could be obtained in the above method was limited to one-half the length of the wave tank. In order to increase that distance, so as to be able to observe the lateral wave well-separated from the reflected wave, a second procedure was adopted. In this case, the wave source was placed near one end of the tank (figure 5*b*). Detectors T_1 and T_2 were placed along a line parallel to the shelf boundary, on the shelf side, at two different distances from the source. The third detector T_3 was again left stationary, on the shelf near the source, to monitor the latter. As a first step, direct waves were once more measured under conditions of uniform depth h_1 throughout the tank, digitized and stored on tape. The floor of the tank was then lowered to h_2 over one full half of the tank and the complete wave field consisting of direct, reflected and lateral waves measured at T_1 and T_2. The direct wave was removed by subtraction, as before. In this case, of course, it was extremely important that the same direct wave should be consistently produced by the source; that this was the case was verified from the output of the monitoring detector T_3. Results obtained from the two experimental procedures were compared over the range of distances where they overlapped: no significant differences were found within the accuracy of measurements.

4. Experimental results

Generated-wave amplitudes were kept as small as possible to remain within the limits of linear theory while also keeping within the bounds of accurate detection. For the experiments described here, wave amplitudes did not exceed 0·4 mm at 1·0 m from the source; a typical wavelength for the leading wave was 15·0 cm. On a shelf of uniform depth $h_1 = 1{\cdot}28$ cm the small parameters which determine the importance of amplitude and phase dispersion are respectively $\epsilon = \eta/h_1 \simeq 0{\cdot}03$ and $\mu = (h_1/\lambda)^2 \simeq 0{\cdot}007$. The Ursell number corresponding to the above values is

$$U = \epsilon/\mu \simeq 4.$$

We use the relation (Whitham 1974, p. 470)

$$\frac{\lambda}{l} = \frac{4}{\sqrt{3}} K(m)$$

to relate the wavelength λ to a more appropriate length scale l for cnoidal waves, with $m = (\eta/h_1)^{\frac{1}{2}}(h_1/l)^{-1}$ varying from $m = 0$ in the linear limit to $m = 1$ for the solitary-wave limit. Substituting for the numerical values and solving for $mK(m) \simeq 0{\cdot}86$ from tables (Abramowitz & Stegun 1965, p. 608) gives $m \simeq 0{\cdot}47$. Thus, within the domain of measurements (distances from the source greater than 1·0 m), the waves

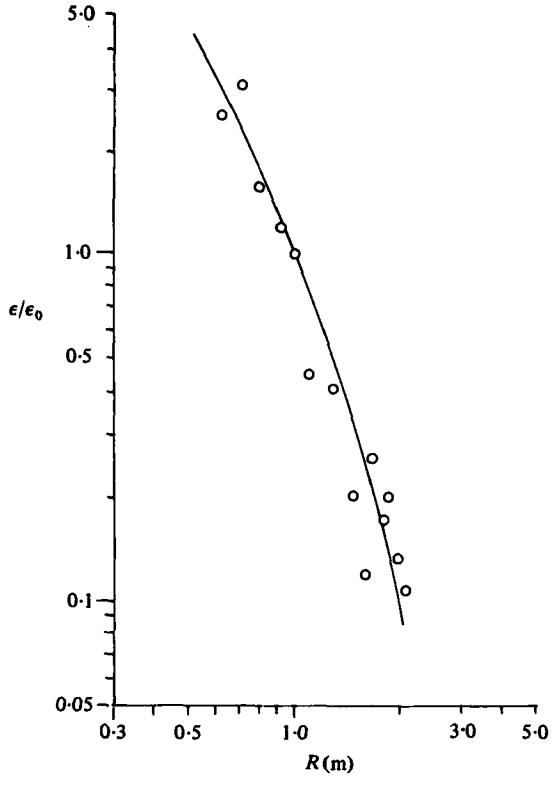

FIGURE 6. Observed spatial energy density of the direct wave (circles), normalized to its value E_0 at a distance of 1·0 m from the source. The continuous curve is the fit given by (5).

generated were long and of infinitesimal amplitude within corrections of order ϵ and μ. The corrections to the propagation speed and to the relations derived at the depth discontinuity are small; this was indeed confirmed by measurements of the direct wave at angles below that of critical incidence ($\theta_c = 49{\cdot}8°$ for the chosen depths).

The only important feature not incorporated in the theoretical framework was that of frictional decay, which showed prominently in the experimental results. Consider for example the energy density of the direct wave $E_D(R)$ which, in the absence of dispersion and friction would be expected to decay as $E_D(R) \sim 1/R$. A glance at figure 6 shows that the decay is more rapid than predicted. Following Pite (1973), a linear bottom-friction model may be used, which predicts

$$E_D(R) \sim \frac{1}{R} e^{-2\alpha_1 R}, \tag{5}$$

where α_1 is the decay coefficient. A least-square fit to our data yields $\alpha_1 \simeq 0{\cdot}75\ \mathrm{m}^{-1}$, in agreement with values found by Pite (1973).

The lateral wave is recognized by its arrival time; over a large portion of the wave tank, on the shelf, it is the first disturbance to reach the detector. An example of the gradual emergence of the lateral wave from the reflected wave is seen in the sequence of traces shown in figure 7. The arrows mark the arrival time of the lateral wave, measured at the first zero-crossing. The observed time of arrival of the lateral wave

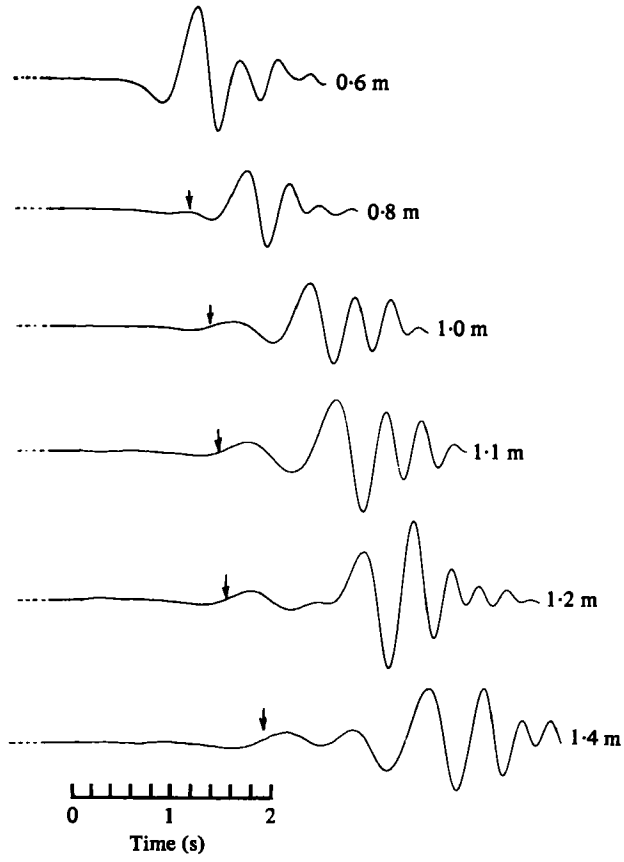

FIGURE 7. The complete wave train, as observed on the shelf at increasing distances from the wave source, showing the emergence of the lateral wave (identified by the arrow showing the first zero-crossing). Wave profiles have been inverted in the data processing: the first disturbance seen in the tank is an elevation (not a depression as shown here). The gain has been increased from trace to trace to remove the decay factor and enhance the similarity between successive traces.

is plotted as a function of distance from the source in figure 8 and seen to correspond very closely with the arrival time predicted by (3). The crossover distance R_c predicted from (4) is 0·82 m; the observed value is $0{\cdot}81 \pm 0{\cdot}02$ m.

The mathematical formulation predicts that the locus of constant phase of the lateral wave is a straight line. Measurements were performed to determine the geometry of the lateral wavefront and the variation of surface amplitude along it. A line of constant phase, according to theory, would be BC' in figure 9. As a matter of convenience, measurements were made along the line BB', which makes an angle of 45° (rather than 49·8°) with the shelf edge. The arrival times along BB' are shown together with theoretical arrival time (solid line); differences average only 2 %. Predicted arrival times along BC' are shown by the dotted line in figure 10. The time $\Delta t = 0{\cdot}12$ s required to travel from B' to C' along a ray making an angle θ_c to the shelf edge is also that found to be the difference in arrival time between waves at B' and the predicted arrival time at C'. The results of the observations confirm the rectilinear shape of the lateral wavefront.

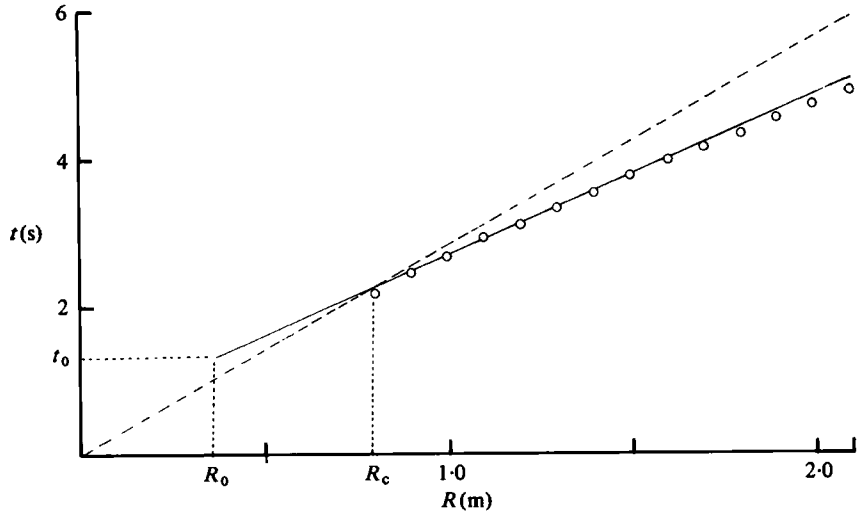

FIGURE 8. Arrival time of the lateral wave (circles) as a function of distance R from the source. The solid line is the arrival time predicted by shallow-water linear theory (3). The dashed line is the arrival time of the direct wave: $t_D = R/c_1$. The lateral wave is seen only for $R_0 > 35$ cm, $t_0 > 1{\cdot}3$ s.

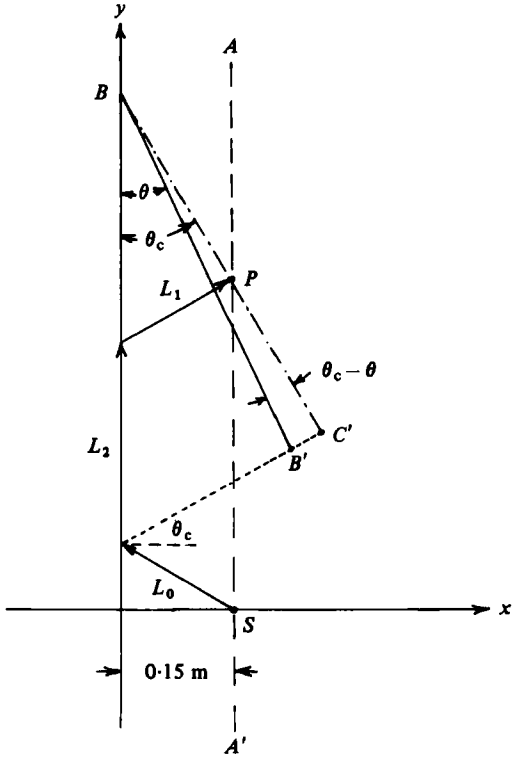

FIGURE 9. Details of the measurement geometry for lateral wave observations described in the text. Here, $\theta_c = 49{\cdot}8°$, $\theta = 45°$.

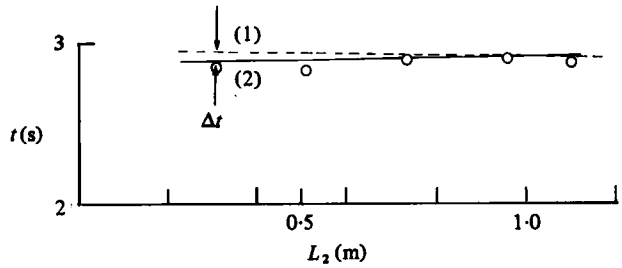

FIGURE 10. Arrival time of the lateral wave along line BB' of figure 9 (circles). The solid line shows the theoretical estimate using (3). The dashed line is the theoretical arrival time along line BC'. The time difference $\Delta t = 0{\cdot}12$ s is also that predicted by theory.

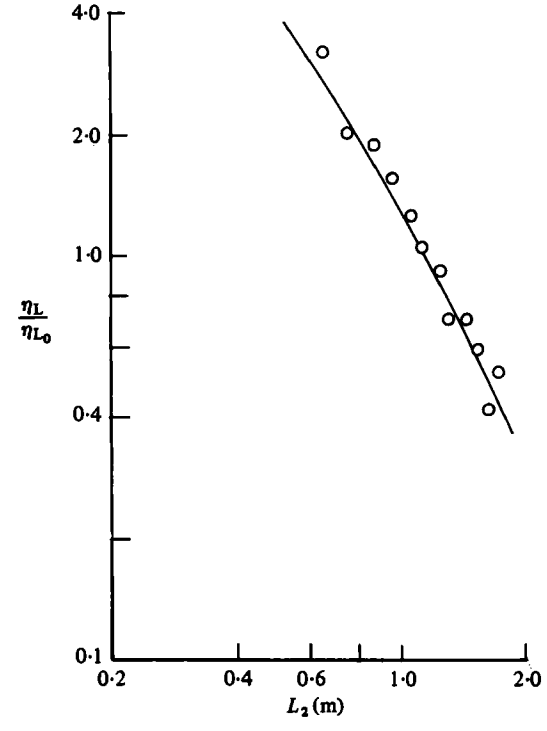

FIGURE 11. The amplitude of the lateral wave (circles), normalized to its value at $R = 1{\cdot}0$ m, as a function of path length L_2 along the shelf edge. The solid line is the theoretical fit given by (6).

Lateral-wave amplitudes were measured along AA' in figure 9, and are shown, normalized to the amplitude at $R = 1$ m, in figure 11. It is clear that the data do not conform to a curve of slope $-\frac{3}{2}$, as predicted by theory, and once again linear friction may be introduced in the equations of motion to predict an exponential damping rate. Noting that at points along AA', i.e. on a line parallel to the shelf edge, path segments L_0 and L_1 are constants and only L_2 increases with distance from the source, we find that with linear friction, the amplitude of the lateral wave should vary along AA' as

$$\eta_L \sim L_2^{-\frac{3}{2}} e^{-\alpha_2 L_2}, \tag{6}$$

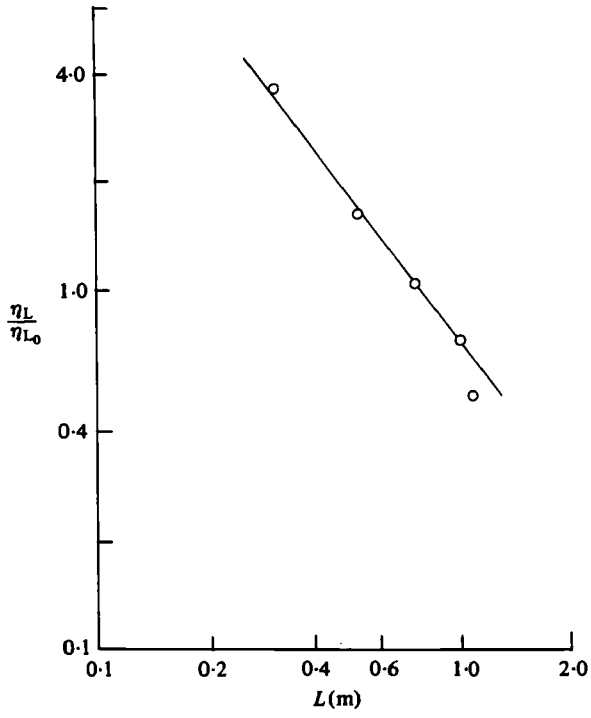

FIGURE 12. Variation of lateral wave amplitude (circles) measured along a wavefront (approximated by line BB' of figure 9) as a function of L_2. The wave amplitude is normalized here with respect to its value at $L_2 = 0{\cdot}745$ m. The solid line is the fit given by (7).

where α_2 is a deep-water frictional-decay coefficient. A least-square fit to the data gives $\alpha_2 \simeq 0{\cdot}32\ \mathrm{m}^{-1}$. Attenuation in deep water is less rapid than in shallow water, as found by Pite (1973).

Measurements of lateral-wave amplitude along the lateral wavefront (made along the line BB' in figure 9, which is a good approximation to the wavefront itself) are best explained by invoking some attenuation along the path segment L_1, which varies along the wavefront as well as along the segment L_2. The fit of the measured points to the curve (figure 12)

$$\eta_L \sim L_2^{-\frac{3}{2}} e^{-(\alpha_1 L_1 + \alpha_2 L_2)}, \tag{7}$$

with α_1 and α_2 taking the values found earlier, is very good and brings attenuation along both deep- and shallow-water path segments into play.

The tank experiments then provide overall confirmation of qualitative as well as quantitative features of the shallow-water linear theory. Propagation times and the shape of the wavefront are accurately predicted by theory; amplitudes are also reproduced provided that some frictional decay is included.

5. Relevance to tsunamis

Inasmuch as the width of the continental slope may not be very small compared to a tsunami wavelength, an abrupt depth discontinuity is not an exact model of the transition from the continental shelf to the deep ocean. In most tsunamigenic areas

of the Pacific Ocean, the width of the continental slope is of the same order as that of the continental shelf, so that only waves produced by sources with dimensions comparable to the shelf width would experience strong reflection at the continental slope. However, since such large sources are the cause of the largest and most important tsunamis, this is not a significant restriction. For a well-documented example of a large source area, the reader is referred to Spaeth & Berkman's (1967) description of the tsunami which followed the 1964 Alaskan earthquake. The presence of a deep trench, such as is commonly seen to be running parallel to the shelf over much of the Pacific Ocean, has not been considered here and might prove important in estimating the time of earliest arrival: the (modified) lateral wave would in that case travel at the deep-water speed corresponding to the trench depth. Finally, the curvature of the oceanic perimeter and of the course of the continental slope is important in the actual ocean on scales of about ten times that of the shelf width.

The question of the relevance of linear shallow-water gravity-wave theory to the description of tsunami propagation also deserves some consideration. Hammack & Segur (1978) have examined the influence of initial conditions on the choice of an effective wave scale l and the possible changes in wave regime as the waves propagate away from their source. Their findings indicate that linear non-dispersive theory is applicable to the leading wave of a long tsunami ($l \simeq 200$ km) in the deep ocean up to a distance of about 60000 km (i.e. effectively anywhere on the Earth) and on continental shelves for propagation distances up to 300 km (i.e. over the whole width of most shelves). For shorter tsunamis ($l \simeq 60$ km), the leading wave may be dispersive before the total width of the shelf is crossed. Direct waves propagating on the shelf itself may travel distances substantially greater than 300 km in shallow water, and the applicability of the linear non-dispersive theory to their very far field is questionable. The lateral wave, by contrast, travels most of its path along the shelf edge, in deep water, and the linear non-dispersive theory should be applicable to its description, as it is to that of deep ocean tsunamis.

We thus have solid grounds to believe that although the theoretical description, as supported by the experimental results in a small-scale model, may not be immediately applicable to any specific tsunami event, it nevertheless provides a basic framework for the interpretation of early tsunami arrivals and perhaps of some of the 'forerunners' referred to in the literature (Murty 1977). In addition, the early arrival time of the lateral wave might bring some modest improvement in tsunami warning schemes.

As an example, consider a short tsunami wave (approx. 15 min period) generated at the midpoint of a 100 km wide shelf that lies adjacent to a deep-water region. Let the depths of the shelf and the deep water be 150 m and 5 km, respectively. For an observation point which, like the source, lies a distance 50 km from the shelf edge, the crossover distance R_c is calculated to be about 125 km downshelf from the source. The waves chosen would have a speed of about 140 km/h and a wavelength of about 35 km. Thus, crossover would occur at a distance of about 3·6 wavelengths. A long tsunami wave (approx. 1·5 h period) would have a wavelength of nearly 200 km and crossover would occur within one wavelength. For communities lying along the shore (100 km from the shelf edge) the point at which the lateral and direct waves would arrive simultaneously (the crossover distance) would be located at a distance $R = 175$ km from the source. It would take these waves 1·25 h to traverse this distance.

For shore communities lying further from the source, the arrival of the lateral wave would precede that of the direct wave. A community located 300 km from the source would record the arrival of the lateral wave at time $t = 1{\cdot}47$ h after generation, whereas the direct wave would arrive after a time $t = 2{\cdot}14$ h, a time difference of 0·67 h. For a community located 500 km from the source, the lateral wave will arrive after time $t = 1{\cdot}75$ h, while the direct wave will arrive after time $t = 3{\cdot}57$ h, a time difference of $t = 1{\cdot}82$ h. We can see that the difference in arrival time of the direct and lateral waves can become significant even over relatively short distances on the oceanic scale. If the lateral wave could be detected and its nature recognized, the differences in arrival times could be used to warn and prepare local populations to take evasive actions in preparation for the oncoming direct and reflected tsunami waves, the amplitudes of which might be quickly estimated from that of their lateral forerunner.

This work was supported by the Natural Sciences and Engineering Research Council of Canada through Operating Grant A 7490. We also thank M. Quick of the Department of Civil Engineering at the University of British Columbia for making available to us space and equipment in his laboratory.

REFERENCES

Abramowitz, M. & Stegun, I. A. 1965 *Handbook of Mathematical Functions*. Dover.

Brekhovskikh, L. M. 1960 *Waves in Layered Media*. Academic.

Cagniard, L. 1939 *Reflection and Refraction of Progressive Seismic Waves*. McGraw-Hill.

Hammack, J. L. & Segur, H. 1978 Modelling criteria for long water waves. *J. Fluid Mech.* **84**, 359–373.

Heelan, P. A. 1953 On the theory of head waves. *Geophysics* **18**, 871–893.

King, D. R. 1978 The wave field on a shelf resulting from point source generation, with application to tsunamis. Ph.D. thesis, University of British Columbia.

Murty, T. S. 1977 *Seismic Sea Waves – Tsunamis*. Dept. of Fisheries and the Environment, Fisheries and Marine Sciences, Ottawa.

Pite, H. D. 1973 Studies in frictionally damped waves. Ph.D. thesis, University of New South Wales.

Spaeth, M. G. & Berkman, S. C. 1967 The tsunami of March 28, 1964, as recorded at tide stations. *U.S. Coast Geodetic Survey Tech. Bull.* no. 23.

Whitham, G. B. 1974 *Linear and Non-Linear Waves*. Wiley.